

ABSTRACT

We report the joint WASP/KELT discovery of WASP-167b/KELT-13b, a transiting hot Jupiter with a 2.02-d orbit around a $V = 10.5$, F1V star with $[\text{Fe}/\text{H}] = 0.1 \pm 0.1$. The $1.5 R_{\text{Jup}}$ planet was confirmed by Doppler tomography of the stellar line profiles during transit. We place a limit of $< 8 M_{\text{Jup}}$ on its mass. The planet is in a retrograde orbit with a sky-projected spin-orbit angle of $\lambda = -165^\circ \pm 5^\circ$. This is in agreement with the known tendency for orbits around hotter stars to be more likely to be misaligned. WASP-167/KELT-13 is one of the few systems where the stellar rotation period is less than the planetary orbital period. We find evidence of non-radial stellar pulsations in the host star, making it a δ -Scuti or γ -Dor variable. The similarity to WASP-33, a previously known hot-Jupiter host with pulsations, adds to the suggestion that close-in planets might be able to excite stellar pulsations.

Key words: techniques: spectroscopic – techniques: photometric – planetary systems – planets and satellites: individual – stars: individual – stars: rotation.

1 INTRODUCTION

There are far fewer hot-Jupiter exoplanets known to transit hot stars with $T_{\text{eff}} > 6700$ K than those transiting later-type stars. This is partially a selection effect given that planets transiting very hot or fast-rotating stars are harder to validate, since the lack of spectral lines makes it harder to obtain accurate radial-velocity measurements. Thus, radial-velocity surveys have tended to avoid hotter stars, while transit searches such as the Wide Angle Search for Planets (WASP) have, in the past, paid less attention to such candidates.

Hot Jupiters are often in orbits that are not aligned with the stellar rotation axis. One explanation is that hot Jupiters migrate within a disc which is itself tilted with respect to the stellar rotation axis, possibly due to a companion (Crida & Batygin 2014; Fielding et al. 2015). Another is that hot Jupiters arrive at their current orbits through high-eccentricity migration, owing to perturbations by third bodies (e.g. Dong et al. 2014), which leads to a range of orbital obliquities.

The planets that have been found around hotter stars have a greater tendency to be in misaligned orbits, compared to planets orbiting later-type stars (Winn et al. 2010; Albrecht et al. 2012), suggesting a systematic difference in their dynamical history. In addition there appears to be a dearth of hot Jupiters orbiting very fast rotators, such that the star rotates faster than the planetary orbit (e.g. Wu & Murray 2003; Fabrycky & Tremaine 2007; McQuillan et al. 2013), though this may again be partially a selection effect. In such stars the usual tidal decay of a hot Jupiter orbit would be reversed, provided the orbit is prograde, again changing the dynamical history.

For such reasons the WASP (Pollacco et al. 2006; Hellier et al. 2011) and KELT (Kilodegree Extremely Little Telescope: Pepper et al. 2007, 2012) transit-search teams are now giving more attention to hotter candidates. The first hot Jupiter found to transit an A-type star was WASP-33b, where the planet was validated, not by radial-velocity measurements, but by the detection of the shadow of the planet seen through tomography of the stellar line profiles during

transit (Collier Cameron et al. 2010b). This technique requires a higher signal-to-noise ratio than radial-velocity measurements, and thus a bigger telescope for a given host-star magnitude.

Tomographic methods have since led to the detection of the hot Jupiters KELT-17b (Zhou et al. 2016), HAT-P-57b (Hartman et al. 2015), XO-6b (Crouzet et al. 2016) and HAT-P-67b (Zhou et al. 2017), as well as the warm Jupiter Kepler-448b (Bourrier et al. 2015). The hot Jupiter Kepler-13 Ab has also been detected tomographically (Johnson et al. 2014), though in that case the planet’s existence had previously been confirmed using the orbital phase curve (Shporer et al. 2011; Mazeh et al. 2012).

In this work we present the joint WASP/KELT discovery of a transiting hot Jupiter dubbed WASP-167b/KELT-13b. The planet host star is a 7000 K, rapidly rotating ($v \sin i_{\star} \approx 50 \text{ km s}^{-1}$) F1V star.

2 DATA AND OBSERVATIONS

WASP-167b/KELT-13b was observed with WASP-South from 2006 May–2012 June and with KELT-South from 2010 March–2013 August. WASP-South is an eight-camera array using 200-mm f/1.8 lenses, covering a $7.8^\circ \times 7.8^\circ$ field of view. Typically eight fields per night were observed with a broadband filter (400–700nm) using 30-s exposures and typically 10-minute cadence. Details of the data reduction and processing are given by Collier Cameron et al. (2006) and an explanation of the process for selecting candidates is given by Collier Cameron et al. (2007).

The KELT-South site consists of a single 80-mm f/1.9 camera with a $26^\circ \times 26^\circ$ field of view and a pixel scale of $23''$. Survey observations use 150-s exposures and a cadence of 10–20 minutes per field. Further details of KELT-South are given in Pepper et al. (2012). Details of the data reduction, processing and candidate selection procedures are given by Siverd et al. (2012) and Kuhn et al. (2016).

The WASP and KELT teams independently found a planet-like transit signal with a ~ 2 -day period (see Fig. 1) and set about obtaining a total of 18 follow-up light curves of the transit. The observations are listed in Table 1 while the lightcurves are shown in Fig. 2. The techniques for obtaining relative photometry have been reported in previous WASP

* E-mail: l.y.temple@keele.ac.uk

and KELT discovery papers, and since we have 18 transit curves from disparate facilities we refer the reader to such papers for full details of the instrumentation and analysis (e.g. Hellier et al. 2014; Maxted et al. 2016; Kuhn et al. 2016; Pepper et al. 2016; Rodriguez et al. 2016). We give key details of the instrumentation used in Table 1.

In an attempt to refute the planetary hypothesis we, on three occasions, attempted to detect an eclipse (of the occulting body by the star) using TRAPPIST with a z' filter (see Table 1 for details). No eclipse was detected, with a 3σ upper limit of 1100 ppm, which is consistent with the occulting body being a planet.

The two teams also began monitoring the radial velocity of the star using the Euler/CORALIE and TRES spectrographs (Queloz et al. 2001; Fűrész 2008). The measured values are listed in Table 2. The crucial tomographic data, revealing the planet shadow, then came from an observation over a transit on the night of March 1st 2016 using the ESO 3.6-m/HARPS spectrograph (Pepe et al. 2002).

We have searched the WASP photometry of WASP-167/KELT-13 for modulations indicating the rotational period of the star, as described by Maxted et al. (2011), but did not find any modulations above ~ 1 mmag.

3 SPECTRAL ANALYSIS

To determine the spectral parameters of the host star we produced a median-stacked spectrum from the 17 HARPS spectra and used it to find the stellar effective temperature T_{eff} , the stellar metallicity [Fe/H], and the projected stellar rotational velocity $v \sin i_{\star}$. The spectra were line-poor and broad-lined, owing to the host star's spectral type, which meant that a determination of the stellar surface gravity $\log g_{\star}$ was not possible. We therefore assume here a value of $\log g_{\star} = 4.3$, the expected value for a similar star at zero age (Gray 1992). The T_{eff} was measured using the H-alpha line, which was strong and unblended. The values obtained for each of these parameters are given in Table 3. Fuller details of our spectral analysis procedure can be found in Doyle et al. (2013). We also used the MKCLASS program (Gray & Corbally 2014) to obtain a spectral type of F1V.

4 PHOTOMETRIC AND RADIAL VELOCITY ANALYSIS

We carried out a Markov Chain Monte Carlo (MCMC) fitting procedure, simultaneously modelling the WASP and KELT light curves, the 18 follow-up light curves, and the out-of-transit RVs. We use the latest version of the code described by Collier Cameron et al. (2007) and Pollacco et al. (2008).

Prior to the fit, the KELT team's follow-up lightcurves were detrended by first fitting them using the online EXOFAST applet (Eastman et al. 2013), removing the effects of airmass and some systematics (this was not needed for TRAPPIST lightcurves). Limb darkening was accounted for using the Claret (2000, 2004) four-parameter non-linear law. At each step of the MCMC the limb-darkening coefficients were interpolated from the Claret tables appropriate to the passband used and the new values of T_{eff} [Fe/H] and $\log g_{\star}$.

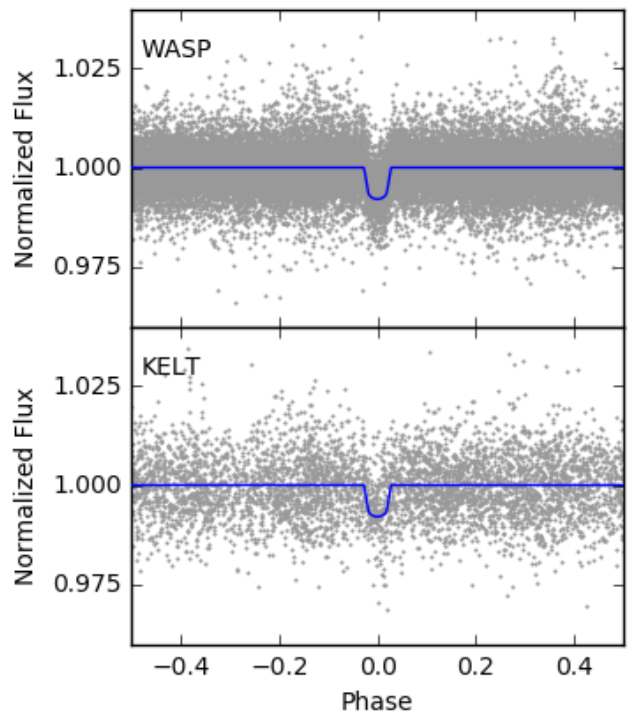


Figure 1. The WASP (top) and KELT (bottom) discovery light curves for WASP 167b/KELT-13b, folded on the orbital period. The blue lines show the final model obtained in the MCMC fitting (see Section 4).

Hot Jupiters settle into a circular orbit on time-scales that are often shorter than their host stars' lifetimes through tidal circularization (Pont et al. 2011). We therefore assume a circular orbit, since this will give the most likely parameters (Anderson et al. 2012).

The system parameters which determine the shape of the transit light curve are: the epoch of mid-transit T_c , the orbital period P , the planet-to-star area ratio $(R_p/R_{\star})^2$ or transit depth δ , the transit duration T_{14} , and the impact parameter b . In the RV modelling, we fit the value of the stellar reflex velocity semi-amplitude K_1 and the barycentric system velocity γ . The proposed values of stellar and planetary masses and radii are constrained by the Enoch-Torres relation (Enoch et al. 2010; Torres et al. 2010). We allow for a possible offset in RVs between the CORALIE and TRES datasets.

Since we collect data from many sources with differing data qualities, our code includes a provision for re-scaling the error bars of each dataset to give $\chi^2_{\nu} = 1$. This means that datasets that don't fit as well are down-weighted, such that the final result is dominated by the better datasets. With 18 transit lightcurves, this means that the final parameters are relatively insensitive to red noise in particular lightcurves.

The radial velocities and the best-fitting model are shown in Figure 3. There is a clear scatter in the RVs about the model, beyond that attributable to the error bars. This could, for example, be caused by the pulsations in the host star (see Section 5) distorting the stellar line profiles, or by a third body in the system. Attempting to fit for a second planet does not properly explain the scatter, but does signif-

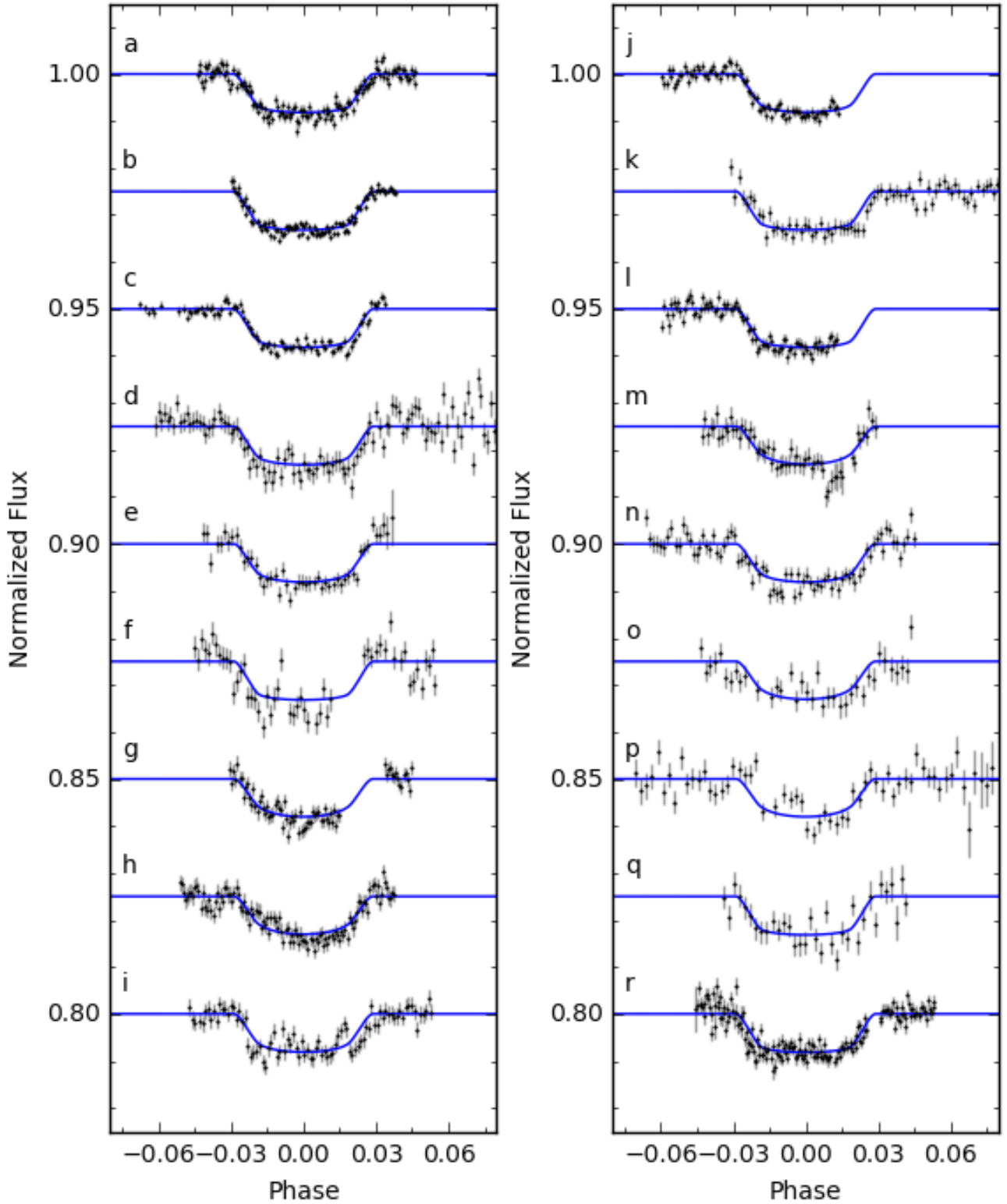


Figure 2. The 18 follow-up transit light curves. The blue lines show the final model obtained in the MCMC fitting (see Section 4). The label to the left of each data set corresponds to an entry in the final column of Table 1.

Table 1. Details of all observations of WASP-167b/KELT-13b used in this work, including the discovery photometry, the follow-up photometry and the spectroscopic observations. The label in the final column corresponds to a lightcurve in Fig. 2.

Facility	Location	Aperture	FOV ($'\times'$)	Pixel Scale ($"\text{pixel}^{-1}$)	Date	Notes	Label
<i>Discovery Photometry</i>							
WASP-South	SAAO ¹ , South Africa	111mm	7.8×7.8	14	2006 May– 2012 Jun	26114 points	-
KELT-South	SAAO, South Africa	42mm	26×26	23	2010 Mar– 2013 Aug	4563 points	-
<i>Transit observations</i>							
TRAPPIST	ESO ² , La Silla, Chile	0.6m	22×22	0.65	2012 Feb 22	I+z'	a
TRAPPIST	ESO, La Silla, Chile	0.6m	22×22	0.65	2012 Apr 30	I+z'	b
LCOGT-LSC	CTIO ³ , Chile	1m	26.5×26.5	0.4	2014 May 17	i'	c
PEST	Perth, Australia	0.3m	31×21	1.2	2014 Jun 22	Rc	d
PEST	Perth, Australia	0.3m	31×21	1.2	2015 Jan 14	V	e
Skynet/Prompt4	CTIO, Chile	0.4m	10×10	0.59	2015 Feb 22	z'	f
T50 Telescope	SSO ⁴ , Australia	0.43m	16.2×15.7	0.92	2015 Mar 24	B	g
T50 Telescope	SSO, Australia	0.43m	16.2×15.7	0.92	2015 Mar 26	B	h
Mt. John	UC ⁵ , New Zealand	0.6m	14×14	0.549	2015 Mar 26	V	i
LCOGT-COJ	SSO, Australia	1m	15.8×15.8	0.24	2015 Mar 28	r'	j
PEST	Perth, Australia	0.3m	31×21	1.2	2015 Mar 28	Ic	k
LCOGT-COJ	SSO, Australia	1m	15.8×15.8	0.24	2015 Mar 28	i'	l
Hazelwood	Victoria, Australia	0.32m	18×12	0.73	2015 Mar 30	B	m
Ivan Curtis	Adelaide, Australia	0.235m	16.6×12.3	0.62	2015 Mar 30	V	n
Ellinbank	Victoria, Australia	0.32m	30.4×14.1	1.12	2015 Apr 03	B	o
PEST	Perth, Australia	0.3m	31×21	1.2	2015 Apr 03	B	p
LCOGT-CPT	SAAO, South Africa	1m	15.8×15.8	0.24	2015 Apr 17	Z	q
TRAPPIST	ESO, La Silla, Chile	0.6m	22×22	0.65	2016 Mar 01	z'	r
<i>Occultation window observations</i>							
TRAPPIST	ESO, La Silla, Chile	0.6m	22×22	0.65	2011 Feb 13	z'	-
TRAPPIST	ESO, La Silla, Chile	0.6m	22×22	0.65	2011 Apr 25	z'	-
TRAPPIST	ESO, La Silla, Chile	0.6m	22×22	0.65	2011 May 09	z'	-
<i>Spectroscopic Observations</i>							
CORALIE	ESO, La Silla, Chile	1.2m	-	-	2010 Apr– 2017 Mar	21 RVs	-
TRES	FLWO ⁶ , Arizona	1.5m	-	-	2015 Feb– 2016 Apr	20 RVs	-
HARPS	ESO, La Silla, Chile	3.6m	-	-	2016 Mar 01	17 CCFs	-

¹South African Astronomical Observatory, ²European Southern Observatory, ³Cerro Tololo Inter-American Observatory, ⁴Siding Spring Observatory, ⁵University of Canturbury, ⁶Fred Lawrence Whipple Observatory

icantly change the semi-amplitude fitted to the first planet. For this reason we do not regard the fitted semi-amplitude as a reliable measure of the planet's mass, but instead report an upper limit of $8 M_{\text{Jup}}$, which we regard as conservative but sufficient to demonstrate that the transiting body has a planetary mass. We are continuing to monitor the system in order to discover the cause of the scatter. The parameters obtained in this analysis are given in Table 3.

5 DOPPLER TOMOGRAPHY

We obtained 17 spectra with the ESO 3.6-m/HARPS spectrograph through a transit on the night of March 1st 2016. We also observed the same transit photometrically using TRAPPIST (see lightcurve r in Fig. 2, Table 1). The standard HARPS Data Reduction Software produces a cross correlation function (CCF) correlated over a window of $\pm 300 \text{ km s}^{-1}$ (as described in Baranne et al. (1996), Pepe et al.

(2002)). The CCFs were created using a binary mask matching a G2 spectral type.

We display the resulting CCFs as a function of the planet's orbital phase in Fig. 4, where phase 0 is mid-transit. In producing this plot we have first subtracted the invariant part of the CCF profile. We do this by constructing a “minimum CCF”, which at each wavelength has the lowest value from the range of phases.

We interpret the CCFs as showing stellar pulsations moving in a prograde direction (moving redward over time). Similar pulsations are seen in the tomograms of WASP-33 (Collier Cameron et al. 2010b; Johnson et al. 2015), which is regarded as a δ -Scuti pulsator (Herrero et al. 2011).

To try to remove the pulsations by separating the features into prograde-moving and retrograde components we followed the method of Johnson et al. (2015), adopted for WASP-33, by Fourier transforming the CCFs. We find that we get the best separation of the components if we do not include the last two spectra in the transform (these two were

Table 2. Radial velocities and bisector spans for WASP-167b/KELT-13b.

BJD (UTC)	RV (km s ⁻¹)	σ_{RV} (km s ⁻¹)	BS (km s ⁻¹)	σ_{BS} (km s ⁻¹)
TRES RVs:				
2457055.9950	-1.01	0.41	-0.12	0.33
2457057.0280	0.00*	0.23	0.03	0.21
2457058.0115	-0.57	0.28	0.53	0.37
2457060.9845	-0.39	0.31	0.33	0.21
2457086.9123	-0.63	0.29	0.04	0.24
2457122.8138	-1.85	0.42	-0.05	0.17
2457123.8544	-1.15	0.39	-0.23	0.28
2457137.7848	-2.39	0.24	-0.29	0.14
2457139.7803	-2.00	0.39	0.15	0.24
2457141.7805	-1.27	0.45	0.17	0.11
2457143.7671	-2.19	0.23	0.17	0.14
2457144.7561	-1.81	0.35	-0.05	0.18
2457145.7548	-1.39	0.32	-0.02	0.16
2457149.7475	-1.16	0.42	0.12	0.25
2457150.7423	-2.33	0.44	0.05	0.20
2457151.7486	-1.19	0.44	-0.20	0.23
2457152.7481	-2.52	0.36	-0.29	0.18
2457406.0418	-1.03	0.34	-	-
2457491.8087	-0.84	0.34	-	-
2457504.7985	-1.62	0.28	-	-
CORALIE RVs:				
2455310.5197	-3.82	0.059	-2.38	0.12
2455310.7997	-3.74	0.061	-0.42	0.12
2455311.8274	-2.83	0.059	-1.30	0.12
2455320.5330	-3.50	0.063	1.80	0.13
2455320.7620	-2.23	0.066	-2.30	0.13
2455568.8071	-2.72	0.060	-2.70	0.12
2455572.8745	-3.09	0.066	-	-
2455574.8560	-3.57	0.061	-4.96	0.12
2455646.7721	-2.51	0.070	-2.96	0.14
2455712.5524	-3.36	0.059	0.26	0.12
2455722.5352	-2.27	0.058	-4.94	0.12
2455979.6808	-3.76	0.062	-3.44	0.12
2455979.8947	-3.74	0.059	-7.50	0.12
2455981.7262	-4.62	0.065	-1.09	0.13
2457600.5003	-4.28	0.071	-	-
2457616.4963	-4.70	0.066	0.048	0.13
2457759.8362	-4.71	0.065	-1.86	0.13
2457760.8358	-3.77	0.066	-3.70	0.13
2457804.7049	-4.08	0.065	-	-
2457809.7742	-5.18	0.064	-2.88	0.13
2457818.6599	-4.73	0.067	-0.25	0.13

* This observation was used as the template for the extraction of the TRES radial velocities.

in any case outside the transit and so cannot contain information about a planet).

Fig. 5 shows the Fourier-transformed data, where the feature running from bottom-left to top-right can be attributed to the pulsations. We thus applied the filter used by Johnson et al. (2015), which contained zeroes in the quadrants containing the prograde pulsation signal and unity in the quadrants containing the retrograde signal, with a Hann function bridging the discontinuity.

We then Fourier transform the masked data back into phase versus velocity and display that in Fig. 6. This shows an apparent retrograde trace, which we attribute to the

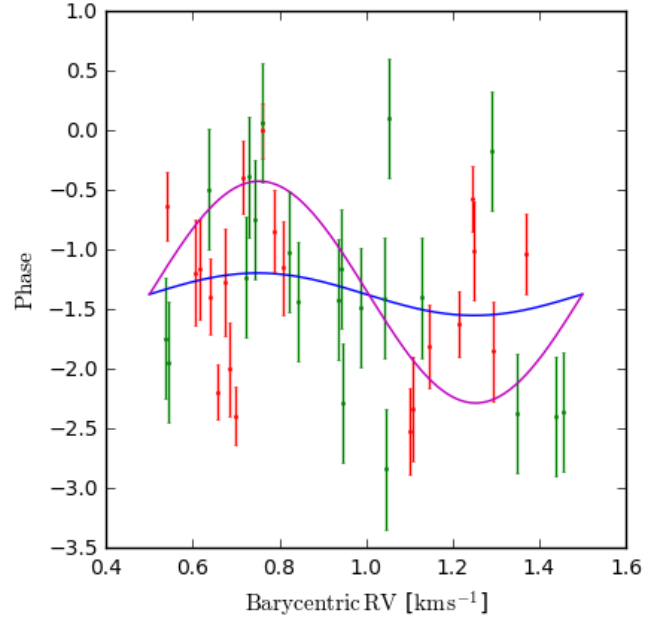


Figure 3. The 21 CORALIE RVs (green) and 20 TRES RVs (red) obtained for WASP-167/KELT-13. The blue line shows the best fitting semi-amplitude, which we do not regard as reliable. The magenta line shows the RV amplitude for a planet mass of $8 M_{Jup}$, which we regard as a conservative upper limit.

shadow of a planet. This is again similar to what is seen in WASP-33 (Johnson et al. 2015).

The planet’s Doppler shadow seems to disappear towards the end of the transit (see Fig. 6). It is likely that it has been reduced during the filtering process, as a result of imperfect separation of the planetary and stellar-pulsation signals. This might have some effect on fitting the alignment angle λ , which depends on the slope of the Doppler shadow, but should have less effect on the other fitted quantities.

In order to parametrise the planet’s orbit we then fitted the CCFs through transit, in a manner similar to the methods in Brown et al. (2017). Since we had subtracted the “minimum CCF” above, we first add that back in to the filtered CCFs in order to reintroduce the stellar line profile, which is a key feature for constraining the value of $v \sin i_{\star}$.

The parameters which define the shape of the CCF line profile are: the projected spin-orbit misalignment angle λ ; the stellar line-profile Full-Width at Half-Maximum (FWHM); the FWHM of the line perturbation due to the planet; the stellar γ -velocity, and $v \sin i_{\star}$. These parameters were fitted using a MCMC fitting algorithm which assumes a Gaussian shape for the line perturbation caused by the planet. The value of $v \sin i_{\star}$ obtained in the spectral analysis was used as a prior in the fit. Initial values for the stellar line FWHM and the γ -velocity were obtained by fitting a Gaussian profile to the CCFs. The λ angle was given no prior. Details of the fitting algorithm are given in Collier Cameron et al. (2010a), and the resulting system parameters are listed in Table 3.

Lastly, in Fig. 7 we show the pulsations without the planet trace, obtained by filtering to leave only the prograde quadrants, and then transforming back into velocity space.

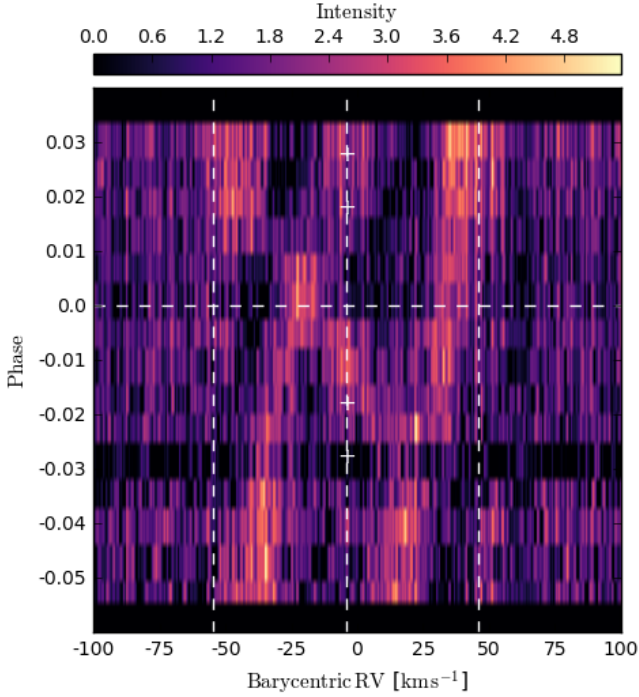


Figure 4. The line profiles through transit. We interpret this as showing prograde moving stellar pulsations and a retrograde moving planet trace. The white dashed vertical lines mark the positions of the γ velocity of the system and the positions of $\gamma \pm v \sin i_*$ (i.e. the centre and edges of the stellar line profile). The phase of mid-transit is marked by the white horizontal dashed line. The white + symbols indicate the four transit contact points, calculated using the ephemeris obtained in the analysis in Section 4.

6 EVOLUTIONARY STATUS

We then used *MINESweeper*, a newly developed Bayesian approach to determining stellar parameters using the MIST stellar evolution models (Choi et al. 2016). Examples of the use of *MINESweeper* in determining stellar parameters are shown in Rodriguez et al. (2017a,b). We model the available B_T , V_T photometry from Tycho-2, J, H, K_s from 2MASS, and WISE W1-3 photometry. We also include in the likelihood calculation the measured parameters from the spectroscopic analysis ($T_{\text{eff}} = 6900 \pm 150$ K and $[\text{Fe}/\text{H}] = -0.04 \pm 0.18$), as well as the *Gaia* DR1 parallax ($\pi = 2.28 \pm 0.62$ mas; Gaia Collaboration et al. (2016b,a)) and the fitted transit stellar density ($0.28 \pm 0.02 \rho_\odot$). We applied non-informative priors on all parameters within the MIST grid of stellar evolution models, and a non-informative prior on extinction (A_V) between 0–2.0 mags. Our final parameters are determined from the value at the highest posterior probability for each parameter, and the errors are based on the marginalized inner-68th percentile range. These are given in Table 4.

For comparison, we also use the open source software *BAGEMASS*¹, which uses the Bayesian method described by Maxted et al. (2015), to estimate the stellar age and mass. The models used in *BAGEMASS* were calculated using the GARSTEC stellar evolution code (Weiss & Schlattl 2008). We use the grid of stellar models in *BAGEMASS* and use the same

¹ <http://sourceforge.net/projects/bagemass>

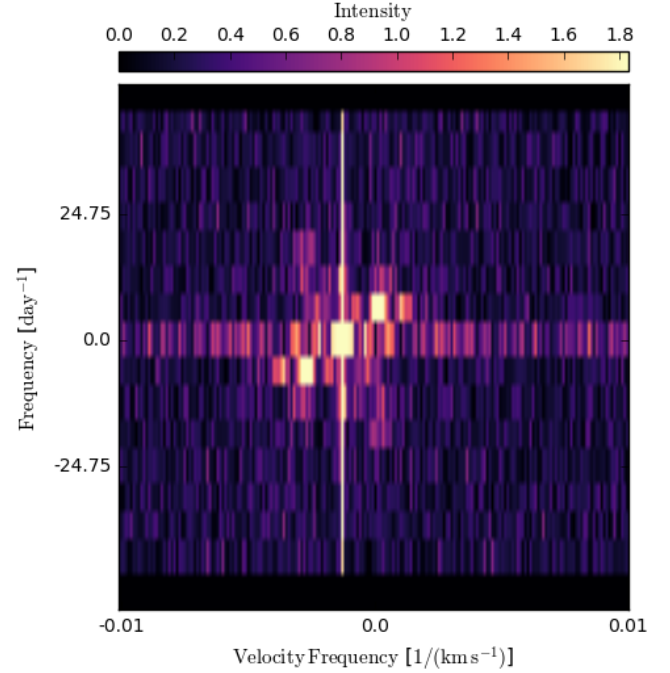


Figure 5. The Fourier transform of the line profiles. The stellar pulsations are seen as the diagonal feature from bottom-left to top-right. The weaker diagonal feature running bottom-right to top-left is produced by the planet.

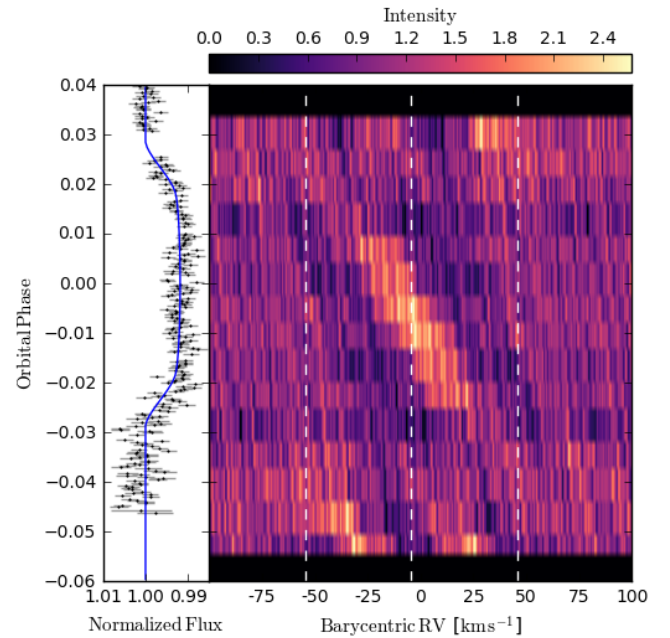


Figure 6. The spectral profiles through transit after removing the stellar pulsations via Fourier filtering. The planet trace is then readily seen moving in a retrograde direction. The left-hand panel shows the simultaneous TRAPPIST photometry of the transit.

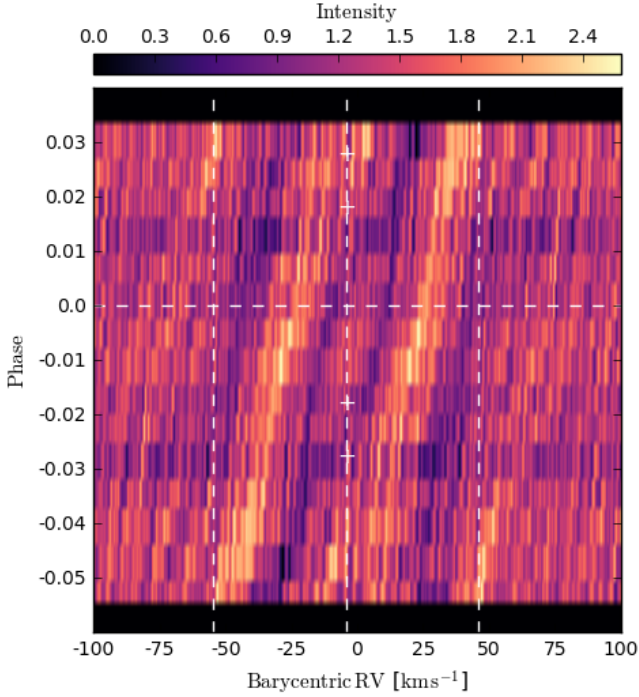


Figure 7. The spectral profiles through transit after removing the planet shadow via Fourier filtering. The stellar pulsations are seen moving in a prograde direction.

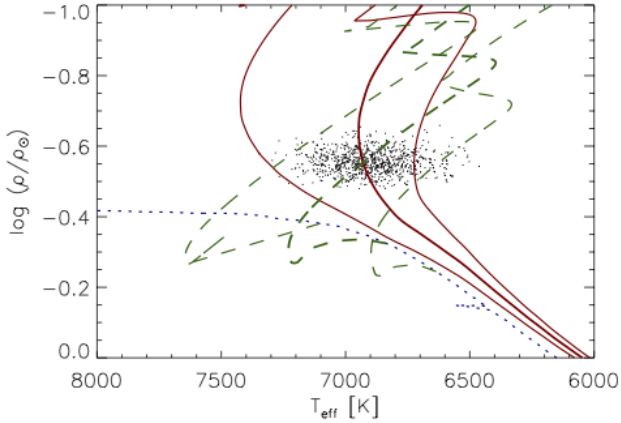


Figure 8. The best fitting evolutionary tracks and isochrones of WASP-167/KELT-13 obtained using BAGEMASS.

temperature, metallicity and density constraints as for the MINESweeper calculation. We also apply a luminosity constraint of $\log L_T = 1.00^{+0.28}_{-0.22}$, which was derived using the *Gaia* parallax and the total line-of-sight reddening as determined by [Schlafly & Finkbeiner \(2011\)](#); [Maxted et al. \(2014\)](#) ($E(B-V) = 0.051 \pm 0.034$). The resulting age and mass values are in Table 4. Both values are compatible with those from MINESweeper. The best-fit stellar evolution tracks and isochrones are shown in Fig. 8.

Table 3. System parameters obtained for WASP-167b/KELT-13b in this work.

1SWASP J130410.53–353258.2
2MASS J13041053–3532582
RA = $13^{\text{h}}04^{\text{m}}10.53^{\text{s}}$, Dec = $-35^{\circ}32'58.28''$ (J2000)
$V = 10.5$
IRFM $T_{\text{eff}} = 6998 \pm 151$ K
<i>Gaia</i> Proper Motions: (RA) -19.031 ± 1.419 mas
Dec) 0.664 ± 1.241 mas/yr
Parallax: 2.28 ± 0.62 mas
Rotational Modulations: < 1 mmag (95%)

Parameter (Unit)	Value
Stellar parameters from spectral analysis:	
T_{eff} (K)	6900 ± 150
$\log A(\text{Fe})$	7.46 ± 0.18
[Fe/H]	-0.04 ± 0.18
$v \sin i_*$ (km s $^{-1}$)	52 ± 8
Parameters from photometry and RV analysis:	
P (d)	2.0219591 ± 0.0000006
T_c (HJD)	2456592.4635 ± 0.0002
T_{14} (d)	0.1133 ± 0.0008
$T_{12} = T_{34}$ (d)	0.021 ± 0.001
$\Delta F = R_p^2/R_*^2$	0.0082 ± 0.0001
b	0.77 ± 0.01
a (AU)	0.0365 ± 0.0006
i ($^{\circ}$)	79.9 ± 0.4
T_{eff} (K)	7000 ± 250
$\log g_*$ (cgs)	4.13 ± 0.02
ρ_* (ρ_{\odot})	0.28 ± 0.02
[Fe/H]	0.1 ± 0.1
M_* (M_{\odot})	1.59 ± 0.08
R_* (R_{\odot})	1.79 ± 0.05
M_p (M_{Jup})	< 8
R_p (R_{Jup})	1.51 ± 0.03
Parameters from tomography:	
γ (km s $^{-1}$)	-3.409 ± 0.007
$v \sin i_*$ (km s $^{-1}$)	49.94 ± 0.04
λ ($^{\circ}$)	-165 ± 5

7 DISCUSSION

7.1 Stellar rotation rate and tidal interaction

As an F1V star with $T_{\text{eff}} = 6900 \pm 150$ K, WASP-167/KELT-13 is among the hottest stars known to host a transiting hot Jupiter. Others include WASP-33 ([Collier Cameron et al. 2010b](#)), Kepler-13 ([Shporer et al. 2011, 2014](#)), KELT-17 ([Zhou et al. 2016](#)) and HAT-P-57 ([Hartman et al. 2015](#)). In addition, WASP-167/KELT-13 appears to be one of the most rapidly rotating stars known to host a hot Jupiter, and one of the few with a stellar rotation period shorter than the planet's orbit. The measured $v \sin i_*$ of 49.94 ± 0.04 km s $^{-1}$ and the fitted radius of $1.79 \pm 0.05 R_{\odot}$ imply a rotation period of $P_{\text{rot}} < 1.81$ days, which compares with the planet's orbital period of 2.02 days.

Thus WASP-167/KELT-13 joins WASP-33 ($P_{\text{orb}} = 1.22$ d; $P_{\text{rot}} < 0.79$ d, [Collier Cameron et al. 2010b](#)), KELT-7 ($P_{\text{orb}} = 2.7$ -d, $P_{\text{rot}} < 1.32$, [Bieryla et al. 2015](#)) and CoRoT-11b ($P_{\text{orb}} = 3.0$ d; $P_{\text{rot}} < 1.73$ d, [Gandolfi et al. 2010](#)) in having a hot Jupiter in a < 3 -d orbit and an even shorter rotation

Table 4. Stellar parameters obtained for WASP-167/KELT-13 in the SED analysis (see Section 6).

Parameter (Unit)	Description	Value
MINESweeper:		
Age (Gyr)	Stellar Age	$1.29^{+0.36}_{-0.27}$
M_* (M_\odot)	Stellar Mass	$1.518^{+0.069}_{-0.087}$
R_* (R_\odot)	Stellar Radius	$1.756^{+0.067}_{-0.057}$
$\log L_*$ (L_\odot)	Log Stellar Luminosity	$0.835^{+0.040}_{-0.034}$
T_{eff} (K)	Effective Temperature	7043^{+89}_{-68}
$\log g_*$	Stellar Surface Gravity	$4.131^{+0.018}_{-0.028}$
$[\text{Fe}/\text{H}]_{\text{surface}}$	Surface Metallicity	$-0.01^{+0.17}_{-0.10}$
$[\text{Fe}/\text{H}]_{\text{init}}$	Metallicity at Formation	$-0.04^{+0.16}_{-0.09}$
Distance (pc)	381^{+15}_{-13}
A_V (mag)	Extinction	$0.044^{+0.057}_{-0.025}$
BAGEMASS:		
Age (Gyr)	Stellar Age	1.56 ± 0.40
M_* (M_\odot)	Stellar Mass	1.49 ± 0.09

rate. See, also, [Crouzet et al. \(2016\)](#) for a discussion of other systems with $P_{\text{rot}} < P_{\text{orb}}$ but with longer period orbits.

The tidal interaction will be different in such systems compared to the more-usual $P_{\text{rot}} > P_{\text{orb}}$. In most hot Jupiters, the tidal interaction is expected to drain angular momentum from the orbit, leading to tidal decay of the orbital period (e.g. [Levrard et al. 2009](#)). This would be reversed, however, for systems with $P_{\text{rot}} < P_{\text{orb}}$, and with the planet in a prograde orbit (such as KELT-7b and CoRoT-11b), thus leading to a different dynamical history.

If, though, $P_{\text{rot}} < P_{\text{orb}}$ and with the planet in a retrograde orbit, such as WASP-167b/KELT-13b or WASP-33b, tidal infall would again be expected. [McQuillan et al. \(2013\)](#) analysed *Kepler* detections and found a dearth of close-in planets around fast rotators, saying that only stars with rotation periods longer than 5–10 days have planets with periods shorter than 3 days. [Teitler & Königl \(2014\)](#) then attributed this to the destruction of close-in planets, with the result of spinning up the star. While WASP-167/KELT-13 and the others just named are examples of systems with $P_{\text{rot}} < P_{\text{orb}}$ they are undoubtedly rare and their dynamics deserves further investigation.

7.2 The retrograde orbit

The planet WASP-167b/KELT-13b has a radius of $1.5 R_{\text{Jup}}$ and is thus inflated, though not exceptionally so. This is in line with WASP-33b, which also has a $1.5 R_{\text{Jup}}$ radius, and is expected for a hot Jupiter orbiting a hot star, given that a relation between inflated radii and stellar irradiation is now well established (e.g. [Demory & Seager 2011](#); [Enoch et al. 2012](#); [Hartman et al. 2016](#)). We should, though, warn of a selection effect against observing non-inflated planets around relatively large A/F stars, in that the transits would be shallower and may escape detection in WASP-like surveys.

[Crouzet et al. \(2016\)](#) list 6 planets with measured sky-projected obliquity angles (λ) that transit host stars hotter

than 6700 K (these are XO-6b, CoRoT-3b, KELT-7b, KOI-12b, WASP-33b & Kepler-13Ab). Of these, five seem to be misaligned but only moderately so, having non-zero λ values with $|\lambda|$ typically 10–40°. WASP-167b/KELT-13b having a highly retrograde orbit with $\lambda = -165^\circ \pm 5^\circ$, now joins the exception WASP-33b, which has $\lambda = -109^\circ \pm 1^\circ$ ([Collier Cameron et al. 2010b](#)).

As has been widely discussed (e.g. [Albrecht et al. 2012](#); [Crida & Batygin 2014](#); [Fielding et al. 2015](#); [Li & Winn 2016](#)), stars hotter than 6100 K host hot Jupiters with a large range of obliquities, whereas cooler stars tend to have planets in aligned orbits (see, e.g., Fig. 8 of [Crouzet et al. \(2016\)](#)). The suggestion is that hotter stars are less effective at tidally damping a planet’s obliquity, perhaps owing to their relatively small convective envelopes (e.g. [Winn et al. 2010](#)). The discovery of WASP-167b/KELT-13b now reinforces this trend.

7.3 Stellar pulsations

WASP-167/KELT-13 is one of a growing number of hot-Jupiter hosts that have shown non-radial pulsations. The first was WASP-33b ([Collier Cameron et al. 2010b](#)), which shows δ -Scuti pulsations with a dominant period near 21 cycles d^{-1} (86 mins) and an amplitude of several mmag ([Kovács et al. 2013](#); [von Essen et al. 2014](#)). Further, [Herrero et al. \(2011\)](#) noted that one of the pulsation frequencies was very near 26 times the orbital frequency of the planet, which suggests that the planet might be exciting the pulsations.

HAT-P-2b is an eccentric massive planet ($8 M_{\text{Jup}}$, $e \sim 0.5$) in a 5-d orbit. [de Wit et al. \(2017\)](#) detect pulsations in *Spitzer* lightcurves of HAT-P-2b, at a level of 40 ppm, much lower than in WASP-33b, but at a similar timescale of ~ 87 mins. Owing to the commensurability between the pulsation and orbital frequencies, [de Wit et al. \(2017\)](#) again suggest that the planet is exciting the pulsations.

A third example is WASP-118, which shows pulsations at a timescale of ~ 1.9 d and an amplitude of ~ 200 ppm in *K2* observations ([Močnik et al. 2017](#)). Another is HAT-P-56, a γ -Dor pulsator with a primary pulsation period of 1.644 ± 0.03 days, which were also seen in *K2* observations ([Huang et al. 2015](#)).

In WASP-167/KELT-13 judging from Fig. 4, the pulsations appear to have a timescale of ~ 4 hours, though with limited data we cannot be more precise. It is possible that some of the transit lightcurves in Fig. 2 are affected by pulsations, but we need more extensive photometry to assess this and to evaluate the pulsation amplitude. Similarly, it may be that pulsations are contributing to the scatter in the RV measurements seen in Fig. 3. Indeed, [de Wit et al. \(2017\)](#) attribute radial-velocity scatter in HAT-P-2 to the pulsations. [Hay et al. \(2016\)](#) also report excess RV scatter in WASP-118.

The pulsations in WASP-167/KELT-13 have a longer timescale than in WASP-33 and HAT-P-2 and are near the borderline between δ -Scuti and γ -Dor behaviour, and so we are unsure which class to assign the star to. We run a second rotational modulation search on the WASP photometry of WASP-167/KELT-13, looking for pulsations at frequencies of 1–50 cycles/day. We do not detect a signal, implying that if the pulsations are present they must have an amplitude of

<500ppm. It is worth noting that both planets WASP-33b and WASP-167b/KELT-13b have retrograde orbits, whereas that of HAT-P-2b is highly eccentric, which may be relevant to the excitation of the pulsations.

ACKNOWLEDGEMENTS

WASP-South is hosted by the South African Astronomical Observatory and we are grateful for their ongoing support and assistance. Funding for WASP comes from consortium universities and from the UK's Science and Technology Facilities Council. The Euler Swiss telescope is supported by the Swiss National Science Foundation. TRAPPIST is funded by the Belgian Fund for Scientific Research (Fond National de la Recherche Scientifique, FNRS) under the grant FRFC 2.5.594.09.F, with the participation of the Swiss National Science Foundation (SNF). M. Gillon and E. Jehin are FNRS Research Associates. We acknowledge use of the ESO 3.6-m/HARPS under program 096.C-0762. L. Delrez acknowledges support from the Gruber Foundation Fellowship.

Work performed by P.A.C. was supported by NASA grant NNX13AI46G. D.J.S and B.S.G. were partially supported by NSF CAREER Grant AST-1056524. S.V.Jr. is supported by the National Science Foundation Graduate Research Fellowship under Grant No. DGE-1343012. Work performed by J.E.R. was supported by the Harvard Future Faculty Leaders Postdoctoral fellowship.

REFERENCES

- Albrecht S., et al., 2012, *ApJ*, **757**, 18
 Anderson D. R., et al., 2012, *MNRAS*, **422**, 1988
 Baranne A., et al., 1996, *A&AS*, **119**, 373
 Bieryla A., et al., 2015, *AJ*, **150**, 12
 Bourrier V., et al., 2015, *A&A*, **579**, A55
 Brown D. J. A., et al., 2017, *MNRAS*, **464**, 810
 Choi J., Dotter A., Conroy C., Cantiello M., Paxton B., Johnson B. D., 2016, *ApJ*, **823**, 102
 Claret A., 2000, *A&A*, **363**, 1081
 Claret A., 2004, *A&A*, **428**, 1001
 Collier Cameron A., et al., 2006, *MNRAS*, **373**, 799
 Collier Cameron A., et al., 2007, *MNRAS*, **380**, 1230
 Collier Cameron A., Bruce V. A., Miller G. R. M., Triard A. H. M. J., Queloz D., 2010a, *MNRAS*, **403**, 151
 Collier Cameron A., et al., 2010b, *MNRAS*, **407**, 507
 Crida A., Batygin K., 2014, in Ballet J., Martins F., Bournaud F., Monier R., Reylé C., eds, SF2A-2014: Proceedings of the Annual meeting of the French Society of Astronomy and Astrophysics. pp 217–220
 Crouzet N., et al., 2016, preprint, ([arXiv:1612.02776](https://arxiv.org/abs/1612.02776))
 Demory B.-O., Seager S., 2011, *ApJS*, **197**, 12
 Dong S., Katz B., Socrates A., 2014, *ApJ*, **781**, L5
 Doyle A. P., et al., 2013, *MNRAS*, **428**, 3164
 Eastman J., Gaudi B. S., Agol E., 2013, *PASP*, **125**, 83
 Enoch B., Collier Cameron A., Parley N. R., Hebb L., 2010, *A&A*, **516**, A33
 Enoch B., Collier Cameron A., Horne K., 2012, *A&A*, **540**, A99
 Fúresz G., 2008, PhD thesis, Univ. Szegeged, Hungary
 Fabrycky D., Tremaine S., 2007, *ApJ*, **669**, 1298
 Fielding D. B., McKee C. F., Socrates A., Cunningham A. J., Klein R. I., 2015, *MNRAS*, **450**, 3306
 Gaia Collaboration et al., 2016a, *A&A*, **595**, A1
 Gaia Collaboration et al., 2016b, *A&A*, **595**, A2
 Gandolfi D., et al., 2010, *A&A*, **524**, A55
 Gray D. F., 1992, The observation and analysis of stellar photospheres.
 Gray R. O., Corbally C. J., 2014, *AJ*, **147**, 80
 Hartman J. D., et al., 2015, *AJ*, **150**, 197
 Hartman J. D., et al., 2016, *AJ*, **152**, 182
 Hay K. L., et al., 2016, *MNRAS*, **463**, 3276
 Hellier C., et al., 2011, in European Physical Journal Web of Conferences. p. 01004 ([arXiv:1012.2286](https://arxiv.org/abs/1012.2286)), [doi:10.1051/epjconf/20101101004](https://doi.org/10.1051/epjconf/20101101004)
 Hellier C., et al., 2014, *MNRAS*, **440**, 1982
 Herrero E., Morales J. C., Ribas I., Naves R., 2011, *A&A*, **526**, L10
 Huang C. X., et al., 2015, *AJ*, **150**, 85
 Johnson M. C., Cochran W. D., Albrecht S., Dodson-Robinson S. E., Winn J. N., Gullikson K., 2014, *ApJ*, **790**, 30
 Johnson M. C., Cochran W. D., Collier Cameron A., Bayliss D., 2015, *ApJ*, **810**, L23
 Kovács G., et al., 2013, *A&A*, **553**, A44
 Kuhn R. B., et al., 2016, *MNRAS*, **459**, 4281
 Levrard B., Winisdoerffer C., Chabrier G., 2009, *ApJ*, **692**, L9
 Li G., Winn J. N., 2016, *ApJ*, **818**, 5
 Maxted P. F. L., et al., 2011, *PASP*, **123**, 547
 Maxted P. F. L., et al., 2014, *MNRAS*, **437**, 1681
 Maxted P. F. L., Serenelli A. M., Southworth J., 2015, *A&A*, **575**, A36
 Maxted P. F. L., et al., 2016, *A&A*, **591**, A55
 Mazeh T., Nachmani G., Sokol G., Faigler S., Zucker S., 2012, *A&A*, **541**, A56
 McQuillan A., Mazeh T., Aigrain S., 2013, *ApJ*, **775**, L11
 Močnik T., Hellier C., Anderson D. R., Clark B. J. M., 2017, preprint, ([arXiv:1702.05078](https://arxiv.org/abs/1702.05078))
 Pepe F., et al., 2002, *The Messenger*, **110**, 9
 Pepper J., et al., 2007, *PASP*, **119**, 923
 Pepper J., Kuhn R. B., Siverd R., James D., Stassun K., 2012, *PASP*, **124**, 230
 Pepper J., et al., 2016, preprint, ([arXiv:1607.01755](https://arxiv.org/abs/1607.01755))
 Pollacco D. L., et al., 2006, *PASP*, **118**, 1407
 Pollacco D., et al., 2008, *MNRAS*, **385**, 1576
 Pont F., Husnoo N., Mazeh T., Fabrycky D., 2011, *MNRAS*, **414**, 1278
 Queloz D., et al., 2001, *The Messenger*, **105**, 1
 Rodriguez J. E., et al., 2016, *AJ*, **151**, 138
 Rodriguez J. E., et al., 2017a, preprint, ([arXiv:1701.03807](https://arxiv.org/abs/1701.03807))
 Rodriguez J. E., et al., 2017b, *ApJ*, **836**, 209
 Schlafly E. F., Finkbeiner D. P., 2011, *ApJ*, **737**, 103
 Shporer A., et al., 2011, *AJ*, **142**, 195
 Shporer A., et al., 2014, *ApJ*, **788**, 92
 Siverd R. J., et al., 2012, *ApJ*, **761**, 123
 Teitler S., Königl A., 2014, *ApJ*, **786**, 139
 Torres G., Andersen J., Giménez A., 2010, *A&ARv*, **18**, 67
 Weiss A., Schlattl H., 2008, *Ap&SS*, **316**, 99
 Winn J. N., Fabrycky D., Albrecht S., Johnson J. A., 2010, *ApJ*, **718**, L145
 Wu Y., Murray N., 2003, *ApJ*, **589**, 605
 Zhou G., et al., 2016, preprint, ([arXiv:1607.03512](https://arxiv.org/abs/1607.03512))
 Zhou G., et al., 2017, preprint, ([arXiv:1702.00106](https://arxiv.org/abs/1702.00106))
 de Wit J., et al., 2017, preprint, ([arXiv:1702.03797](https://arxiv.org/abs/1702.03797))
 von Essen C., et al., 2014, *A&A*, **561**, A48

This paper has been typeset from a $\text{\TeX}/\text{\LaTeX}$ file prepared by the author.